Floquet Topological Insulators

Muthu Arivoli, Norah Tan, and Chongbin Zheng

May 2019

1 Introduction

1. SHH/Haldane model and ribbon geometry
    - Bloch's theorem
    - Bulk states and edge states
    - Bulk-edge correspondence: relationship between Chern number and edge states
2. Rudner Model and time-dependent Hamiltonian
    - Floquet theory
    - quasienergy and H_{eff}
    - Floquet spectrum
    - winding number
3. From tight-binding to PDE
    - General introduction to these two models
    - tight-binding polarized light model
    - PDE polarized light model

In this paper we study the eigenvalue spectra, edge states, and bulk-boundary correspondence in various models of topological insulators. We start by looking at the Su-Schrieffer-Heeger(SSH) model [7], which describes a one-dimensional chain of atoms with staggered hopping amplitudes. We see that the existence of edge states in the model is related to a topological invariant of the bulk called the winding number. Then we will look at the Haldane model [3], a two-dimensional tight-binding model in a hexagonal lattice. Again, we find a topological invariant called the Chern number associated with the edge states. With a nonzero Chern number, two curves emerge from the upper and lower bands, which are otherwise gapped, and cross over at zero, making the material conduct electricity on the edge. After this we investigate Floquet topological insulators, a group of materials that behave like topological insulators from the application of periodic driving. We examine two models, the Rudner model [6] and the graphene-light [5] model. For each, we study their Floquet spectra, the equivalent of eigenvalue spectra, and construct corresponding topological invariants to study the edge states. Finally, we study a full PDE model of graphene without making the tight-binding approximation. It is the subject of ongoing work to study a full PDE model of the graphene-light system and confirm topological insulator-like behavior without making a tight-binding approximation.

2 The Su-Schrieffer-Heeger(SSH) Model

The first model we will look at is the Su-Schrieffer-Heeger (SSH) model. This is a tight-binding model describing electrons in a one-dimensional atomic chain [7, 1]. Through this relatively simple model, we will illustrate important concepts in the study of topological insulators, such as Bloch theory, edge states, and bulk-edge correspondence. Then, we will apply these concepts to more interesting cases to see that certain properties of a system are solely dependent on some topological invariants of the system.

2.1 The Model

The SSH model arises from the study of polyacetylene, a long one-dimensional polymer that are constructed by the same repeating unit $(C_2H_2)_n$. Applying the tight-binding approximation, the SSH model essentially describes electrons hopping between atoms with staggered amplitudes. Each fundamental cell consists of two atoms next to each other, and the whole system can be constructed by translating the cell in space. The two atoms are located on the A and B sites, respectively. A pictorial illustration of the SSH model is shown in Figure 1. We define the intracell hopping

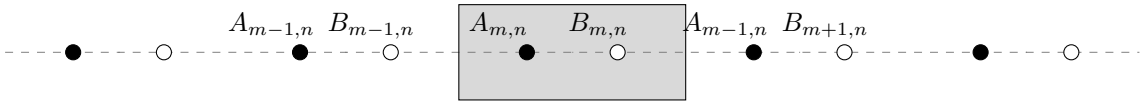

Figure 1: Lattice Structure in the SSH Model. The gray box represents one fundamental cell. The black points are the A sites and the white points the B cites.

amplitude (hopping within the cell) to be t_1 and intercell hopping amplitude to be t_2. The wave function of the n-th fundamental cell can be represented by a vector

$$\psi_n = \begin{pmatrix} \psi_n^A \\ \psi_n^B \end{pmatrix}, \tag{2.1}$$

where ψ_n^A and ψ_n^B represent the value of the wavefunction at the A and B sites, respectively. Therefore, the wavefunction ψ of an electron in a system of N fundamental cells can be described by a vector with length $2N$. Let

$$\psi = (\psi_1^A, \psi_1^B, \psi_2^A, \psi_2^B, ..., \psi_N^A, \psi_N^B)^T. \tag{2.2}$$

From the tight-binding approximation, the Hamiltonian of the system reflects the electron hopping from nearest neighbors. For $N = 3$, the Hamiltonian is the following

$$H_{periodic} = \begin{pmatrix} 0 & t_1 & 0 & 0 & 0 & t_2 \\ t_1 & 0 & t_2 & 0 & 0 & 0 \\ 0 & t_2 & 0 & t_1 & 0 & 0 \\ 0 & 0 & t_1 & 0 & t_2 & 0 \\ 0 & 0 & 0 & t_2 & 0 & t_1 \\ t_2 & 0 & 0 & 0 & t_1 & 0 \end{pmatrix}, \tag{2.3}$$

where we took the periodic boundary condition $\psi_{-1} = \psi_N$ and $\psi_1 = \psi_{N+1}$. We can consider this to be a material that wraps around itself like a loop. When $N \to \infty$, this condition corresponds to an infinite long atomic chain. When the chain is cut off in both directions, the Hamiltonian instead looks like

$$H_{edge} = \begin{pmatrix} 0 & t_1 & 0 & 0 & 0 & 0 \\ t_1 & 0 & t_2 & 0 & 0 & 0 \\ 0 & t_2 & 0 & t_1 & 0 & 0 \\ 0 & 0 & t_1 & 0 & t_2 & 0 \\ 0 & 0 & 0 & t_2 & 0 & t_1 \\ 0 & 0 & 0 & 0 & t_1 & 0 \end{pmatrix}. \tag{2.4}$$

2.2 Bloch Theory

In all the models we study in this paper, the material possesses periodicity in space in one or two directions. Bloch theory makes use of this periodicity and simplifies the problem under investigation.

Suppose we have a one-dimensional periodic material with n fundamental cells separated by distance a. Define T_a to be the translation operator that takes a wavefunction and translate the function to the left by a, namely,

$$T_a\psi(x) = \psi(x + a). \tag{2.5}$$

Since the system is periodic, T_a commutes with the Hamiltonian of the system

$$H = -\frac{1}{2}\partial_x^2 + V(x). \tag{2.6}$$

Therefore, the eigenvalues and eigenvectors of the translation operator can be chosen to be the same as those of Hamiltonian. The eigenvalue problem for the translation operator gives

$$\psi(x+a) = Z\psi(x), \tag{2.7}$$

where Z is corresponding eigenvalue. Now if we apply T_a to $\psi(0)$ for N times, we get

$$\psi(0+Na) = \psi(Na) = Z^N\psi(0). \tag{2.8}$$

If $|Z| \neq 1$, then in the case when $|Z| > 1$, $\psi(Na)$ would approach infinity as $N \to \infty$. When $|Z| < 1$, $\psi(Na)$ would again diverge as $N \to -\infty$. Therefore, $|Z| = 1$, which could be represented by the complex exponential e^{ika} for some real valued k. Thus, we can find all eigenvalues of the Hamiltonian by solving the family of eigenvalue problems

$$-\frac{1}{2}\partial_x^2\psi + V(x)\psi = E\psi, 0 \leq x \leq a \tag{2.9}$$

$$\psi(a) = e^{ika}\psi(0), 0 \leq k \leq \frac{2\pi}{a} \tag{2.10}$$

2.3 Edge States, Winding Number, and Bulk-boundary Correspondence

With Bloch theory we can now greatly simplify the analysis of the SSH model when the system is periodic in space. Since we can study the Schrödinger equation only in one fundamental cell, for the periodic case the Hamiltonian is reduced to

$$H = \begin{pmatrix} 0 & t_1 + t_2e^{-ik} \\ t_1 + t_2e^{ik} & 0 \end{pmatrix}. \tag{2.11}$$

In addition, the periodic boundary condition requires that

$$\begin{aligned} \psi_{-1} &= \psi_N, \\ \psi_{-1} &= e^{ikN}\psi_{-1}, \\ kN &= 2n\pi, \end{aligned} \tag{2.12}$$

or

$$k = \frac{2n\pi}{N} \qquad \text{for } n = 0, 1, .., N-1. \tag{2.13}$$

Therefore, by applying Bloch theory we can calculate the eigenvalue spectrum of the Hamiltonian by solving the eigenvalues of the 2×2 Hamiltonian for each fundamental cell, while taking different values of k based on the boundary conditions. For the aperiodic case, however, such simplification breaks down because of the non-periodic behavior on the edge, and we have to tackle the Hamiltonian directly. We varied the ratio between t_2 and t_1 to study how these parameters affect the eigenvalue spectrum. The eigenvalue spectra for the periodic and aperiodic condition are shown in Figure 2a and 2b, respectively. We can see that for the aperiodic case, two eigenvalues close to 0 appears when $\frac{t_2}{t_1} > 1$. When N is large, these two eigenvalues are so small that we can essentially take them to be zero. Now suppose that we cut off the atomic chain on the left but not on the right. Then we get

$$\begin{pmatrix} 0 & t_1 & & & \\ t_1 & 0 & t_2 & & \\ & t_2 & 0 & t_1 & \\ & & t_1 & 0 & \\ & & & & \ddots \end{pmatrix} \begin{pmatrix} \psi_0^A \\ \psi_0^B \\ \psi_1^A \\ \psi_1^B \\ \vdots \end{pmatrix} = \begin{pmatrix} 0 \\ 0 \\ 0 \\ 0 \\ \vdots \end{pmatrix}, \tag{2.14}$$

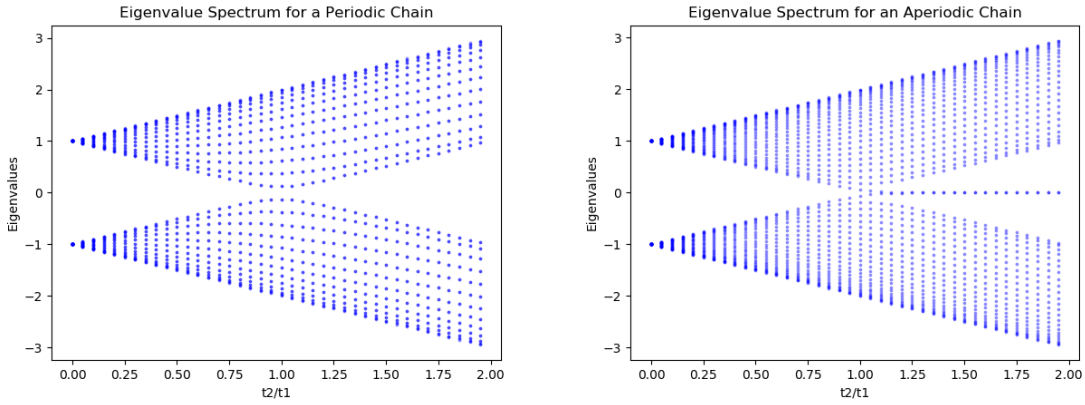

(a) The periodic case (b) The aperiodic case

Figure 2: Eigenvalue spectra of different hopping amplitudes for the SSH model

which means that

$$\begin{aligned} \psi_0^B &= 0, \\ \psi_n^B &= (-\frac{t_2}{t_1})^n \psi_0^B = 0, \\ \psi_0^A &= (-\frac{t_1}{t_2})^n \psi_0^A. \end{aligned} \tag{2.15}$$

This quantitative argument shows that when $t_2 > t_1$, the eigenvectors for the near-zero eigenvalues decay to the right when n is increased. When both sides are cut off, we numerically solved the eigenvectors of the near-zero eigenvalues, which are shown in Figure 14b and 3b. When N is large,

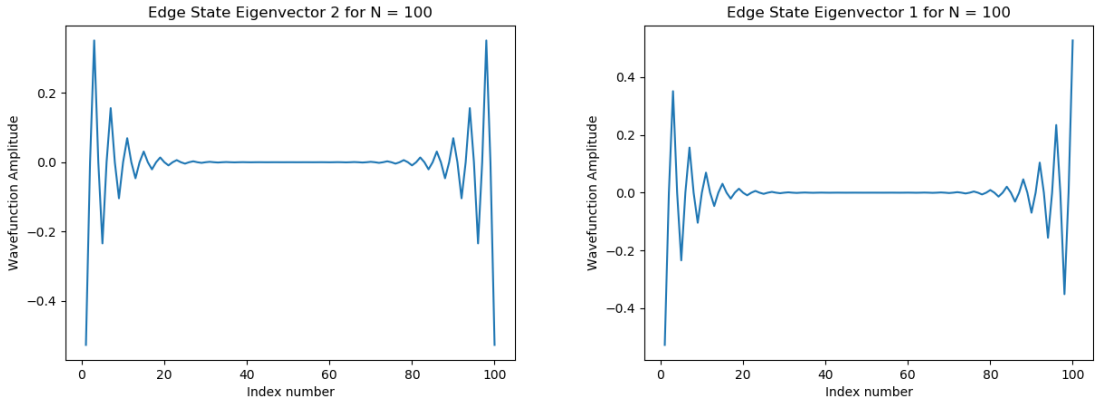

(a) (b)

Figure 3: Edge States of the SSH model. The wavefunction decays when they go away from the edges.

these eigenvectors decay when they get further towards the center and only have significant values around the edges, rather than oscillating across the atomic chain. Thus, we call these special solutions *edge states*.

The existence of the edge states reflect the fact that the system is finite and has well-defined edges. However, only by taking certain parameters do these edge states appear in the solutions. Interestingly, their appearance is closely related to a topological invariant of the bulk properties t_1

and t_2, called the *winding number*. It is defined as the number of times that the curve $t_1 + t_2 e^{ik}$ passes around the origin. As shown in Figure 4, when $t_2 < t_1$, the circle does not contain the

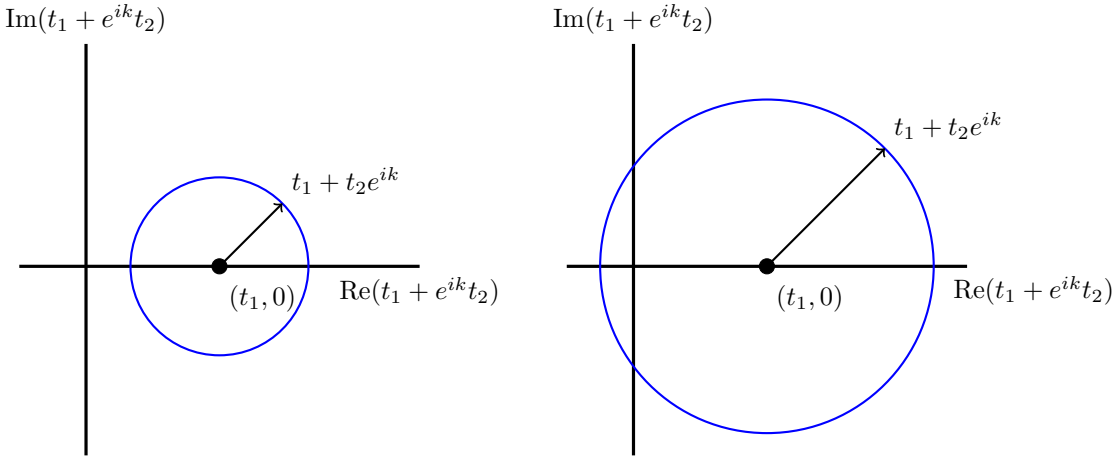

(a) $t_1 > t_2$ (b) $t_1 < t_2$

Figure 4: The curve $t_1 + t_2 e^{ik}$ in the complex plane. It is a circle centered at $(t_1, 0)$ with radius t_2. This figure shows two different possibilities. For 4a, the winding number is zero, and there is no edge state. For 4a, the winding number is one, and edge states exist.

origin, and the winding number is 0. When $t_2 > t_1$, the origin is enclosed by the circle. As we vary k, we go around the circle once, which makes the winding number equal to 1. Therefore, when the winding number is 0, we do not get edge states. When the winding number is 1, we get edge states. In this way, a topological invariant of the system's bulk properties is connected with bahavior that is determined by its edge. This is called *bulk-boundary correspondence*, an important concept that we will return to again and again later in our discussion.

3 The Haldane Model

3.1 The Model

In this section we study the Haldane model, an extension of the tight-binding SSH model to describe electrons hopping in a hexagonal lattice [3]. The lattice structure is shown in Figure 5. Each fundamental cell consists of two sites, denoted as A site and B site, respectively. For each site, the model includes electron hopping from neighboring sites, complex hopping from next-to-nearest neighbors, and an on-site potential V_A or V_B. To get the full system, we can move the fundamental cell in the two directions defined by the basis

$$\vec{v}_1 = \frac{1}{2}(3, -\frac{\sqrt{3}}{2}), \quad \vec{v}_2 = \frac{1}{2}(3, \frac{\sqrt{3}}{2}). \tag{3.1}$$

The system is periodic in these two directions, so Bloch Theorem applies. With the subscripts denoting the indices on the $\vec{v}_1, \vec{v}_2$ directions respectively, Bloch theory tells us that

$$\psi_{m+1,n} = e^{ik_1}\psi_{m,n}, \psi_{m,n+1} = e^{ik_2}\psi_{m,n}. \tag{3.2}$$

The Hamiltonian acting on one fundamental cell is given by

$$\begin{aligned}(H\psi)_{m,n} = t \begin{pmatrix} \psi^B_{m,n} + \psi^B_{m-1,n} + \psi^B_{m,n-1} \\ \psi^A_{m,n} + \psi^A_{m+1,n} + \psi^A_{m,n+1} \end{pmatrix} + \begin{pmatrix} V\psi^A_{m,n} \\ -V\psi^B_{m,n} \end{pmatrix} \\ - t' \begin{pmatrix} e^{i\phi}(\psi^A_{m,n+1} + \psi^A_{m-1,n} + \psi^A_{m+1,n-1}) + e^{-i\phi}(\psi^A_{m,n-1} + \psi^A_{m+1,n} + \psi^A_{m-1,n+1}) \\ e^{i\phi}(\psi^B_{m,n-1} + \psi^B_{m+1,n} + \psi^B_{m-1,n+1}) + e^{-i\phi}(\psi^B_{m,n+1} + \psi^B_{m-1,n} + \psi^B_{m+1,n-1}) \end{pmatrix}.\end{aligned} \tag{3.3}$$

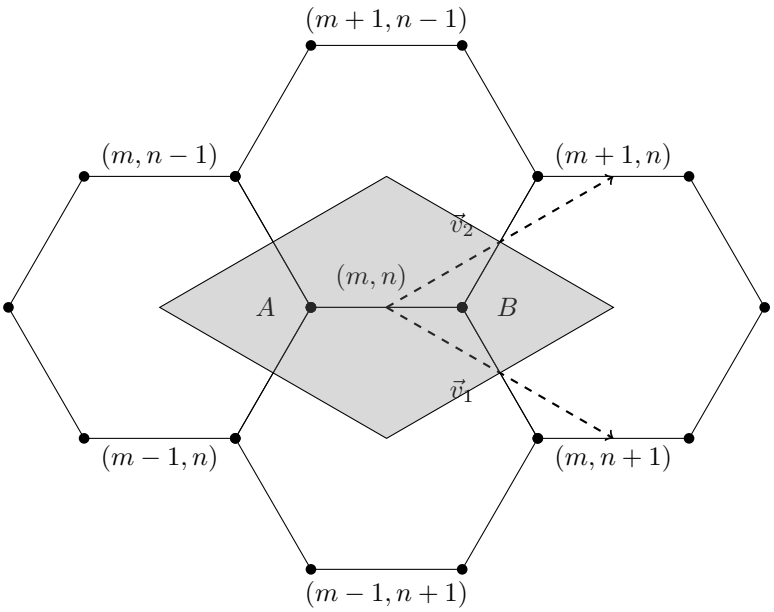

Figure 5: Lattice Structure in the Haldane Model. The gray rhombus represents one fundamental cell. The black points are the A sites and the white points the B sites. We use the coordinates (m, n) to index the fundamental cells in the in the $\vec{v}_1$ and $\vec{v}_2$ directions.

By applying the periodic boundary conditions given by the Bloch Theorem, we can simplify the Hamiltonian as

$$H = \begin{pmatrix} V + t'e^{i\phi}(e^{ik_2} + e^{-ik_1} + e^{i(k_1-k_2)}) + c.c. & t(1 + e^{-ik_1} + e^{-ik_2}) \\ t(1 + e^{ik_1} + e^{ik_2}) & -V + t'e^{i\phi}(e^{-ik_2} + e^{ik_1} + e^{i(k_2-k_1)}) + c.c. \end{pmatrix}, \tag{3.4}$$

where *c.c.* represent the complex conjugate of the term immediately before it.

Now we have reduced the dimension of the problem. To get the eigenvalues of the bulk Hamiltonian, all we need to do is to solve the eigenvalues of the 2×2 matrix here by varying k_1 and k_2 over the interval $[0, 2\pi)$. Note here that we can actually solve the eigenvalues analytically as functions of k_1 and k_2. Expanding the complex exponential using Euler's formula, we can rewrite the Hamiltonian in terms of the Pauli matrices as

$$\begin{aligned} H(k_1, k_2) =& 2t' \cos\phi\big[\cos k_1 + \cos k_1 + \cos(k_1 - k_2)\big] I && (3.5) \\ &+ t(1 + \cos k_1 + \cos k_2)\sigma_1 + t(\sin k_1 + \sin k_2)\sigma_2 && (3.6) \\ &+ \big[V + 2t' \sin\phi(\sin k_1 - \sin k_2 + \sin(k_1 - k_2))\big]\sigma_3, && (3.7) \end{aligned}$$

where I is the identity matrix and σ_1, σ_2 and σ_3 are Pauli matrices:

$$\sigma_1 = \begin{pmatrix} 0 & 1 \\ 1 & 0 \end{pmatrix}, \quad \sigma_2 = \begin{pmatrix} 0 & -i \\ i & 0 \end{pmatrix}, \quad \sigma_3 = \begin{pmatrix} 1 & 0 \\ 0 & -1 \end{pmatrix}. \tag{3.8}$$

For a 2×2 matrix A that can be written in the form

$$A = a\sigma_1 + b\sigma_2 + c\sigma_3 + dI, \qquad a, b, c, d \in \mathbb{R}. \tag{3.9}$$

its eigenvalues are given by

$$\lambda = \pm\sqrt{a^2 + b^2 + c^2} + d. \tag{3.10}$$

Degeneracy of the eigenvalues, therefore, corresponds to the Dirac points at which the two bands touch each other. This occurs when

$$\sqrt{a^2 + b^2 + c^2} = 0. \tag{3.11}$$

Since a, b, c are all real, each of them must be zero. This means that

$$\begin{aligned} t(1 + \cos k_1 + \cos k_2) &= 0, \\ t(\sin k_1 + \sin k_2) &= 0, \\ V + 2t' \sin\phi(\sin k_1 - \sin k_2 + \sin(k_1 - k_2)) &= 0. \end{aligned} \tag{3.12}$$

If we only look at the first two equations, for $t \neq 0$, there are two sets of solutions for (k_1, k_2) at $(\frac{2\pi}{3}, \frac{4\pi}{3})$ and $(\frac{4\pi}{3}, \frac{2\pi}{3})$. For the third equation, for nonzero V, t' and $\sin\phi$, we can solve for the relationship between these variables by plugging in the two points. From this substitution we get

$$V = \pm 3\sqrt{3}t' \sin\phi. \tag{3.13}$$

If the potential V, the hopping amplitude t', and the phase ϕ corresponds to the above equation, we would see the bands touching at either $(\frac{2\pi}{3}, \frac{4\pi}{3})$ or $(\frac{4\pi}{3}, \frac{2\pi}{3})$. If $V = \sin\phi = 0$ or $V = t' = 0$, then we would see both points as Dirac points. Otherwise, the gap between the two bands remain open in the entire region. Numerical solutions of the eigenvalue spectrum, shown in Figure 6, confirms this result.

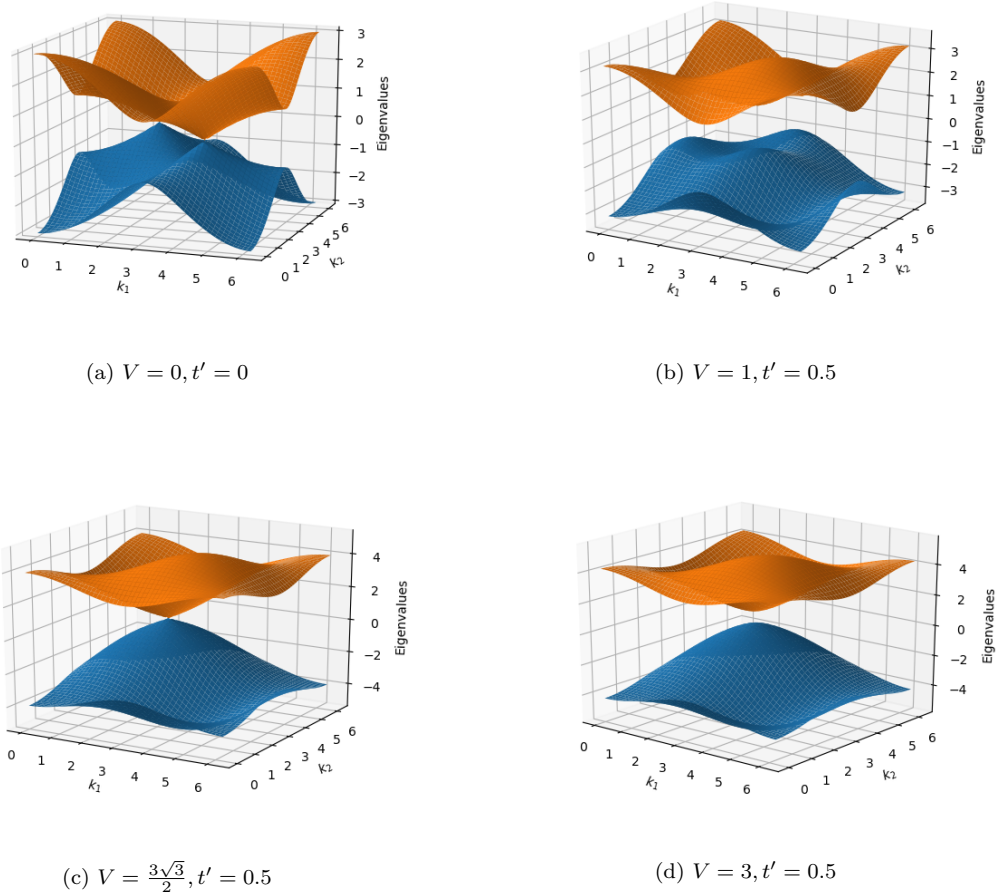

(a) $V = 0, t' = 0$

(b) $V = 1, t' = 0.5$

(c) $V = \frac{3\sqrt{3}}{2}, t' = 0.5$

(d) $V = 3, t' = 0.5$

Figure 6: Eigenvalue spectrum of the Haldane model in the 2-dimensional periodic case. For all four plots the complex hopping phase ϕ is set to be $\frac{\pi}{2}$.

3.2 Edge States and Chern Number

Just like what we did with the SSH model, we now study the effects of edges on the eigenvectors of the system. In the previous section we applied periodic boundary conditions to both directions.

Here, we will keep the periodicity in one direction but cut off the material in another, forming what we call the ribbon geometry. Suppose that there are M fundamental cells in the $\vec{v}_1$ direction and N fundamental cells in the $\vec{v}_2$ direction. $\phi_{m,n}$ represents the wavefunction for the m-th cell in $\vec{v}_1$ and the n-th cell in $\vec{v}_2$, where m runs from 0 to $M-1$ and n runs from 0 to $N-1$. The boundary conditions for the ribbon geometry is

$$\begin{aligned} \psi_{M,n} = \psi_{0,n}, \quad \psi_{-1,n} = \psi_{M-1,n} \qquad & \text{for all } n, \\ \psi_{m,-1} = \psi_{m,N} = 0 \qquad & \text{for all } m, \end{aligned} \tag{3.14}$$

Now although Bloch theory no longer applies in the $\vec{v}_2$ direction, it remains applicable in the $\vec{v}_1$ direction. We can still reduce the Hamiltonian to a $2N \times 2N$ matrix and solve the eigenvalues by varying k_1. The eigenvalue spectrum under the same set of parameters as in Figure 6 are shown in Figure 7. We see that for certain sets of parameters, we get eigenvalues that are close to zero. The

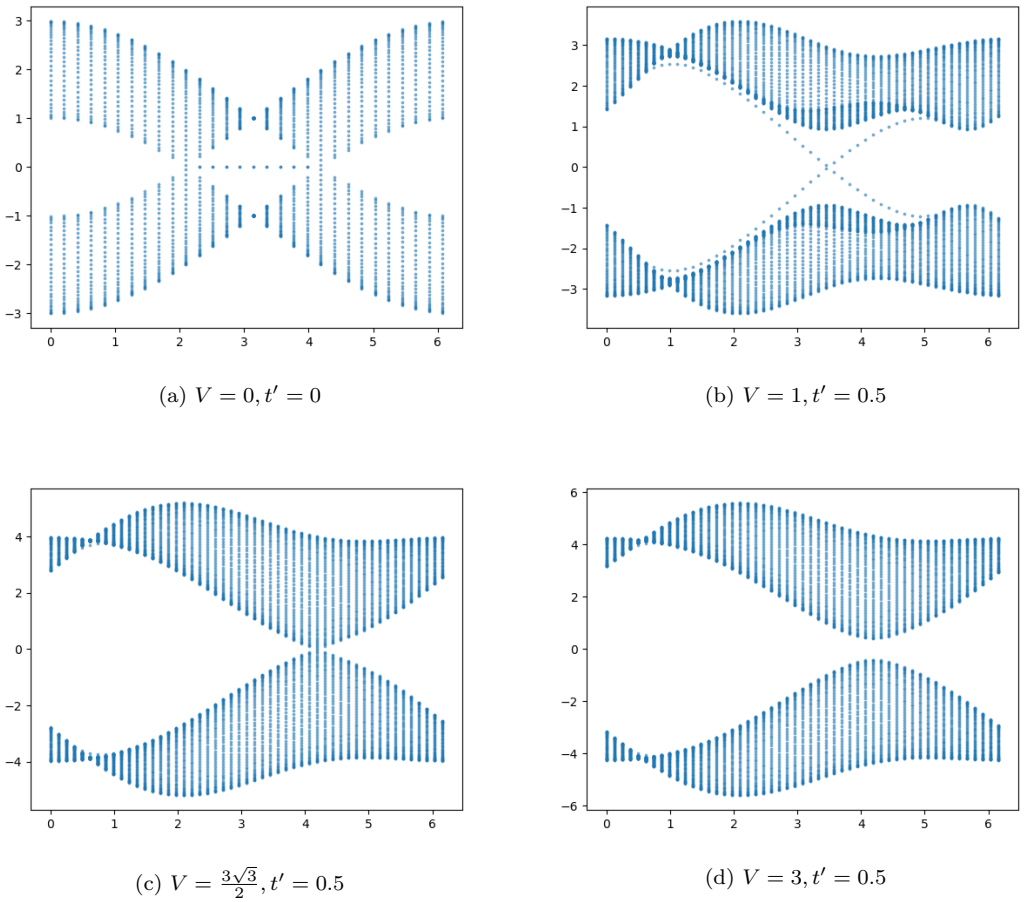

(a) $V = 0, t' = 0$

(b) $V = 1, t' = 0.5$

(c) $V = \frac{3\sqrt{3}}{2}, t' = 0.5$

(d) $V = 3, t' = 0.5$

Figure 7: Eigenvalue spectrum of the Haldane model in the ribbon geometry. For all four plots the complex hopping phase $\phi = \frac{\pi}{2}$.

corresponding eigenvectors of these eigenvalues are the edge states in the ribbon geometry. For example, for the parameters in 7b, two of the edge states is shown in Figure 8. The wavefunction only have significant values around the edge and decays quickly as it gets further from the edge, which is similar to what we have seen in the SSH model.

As it turns out, there is also a topological invariant associated with the existence of the edge

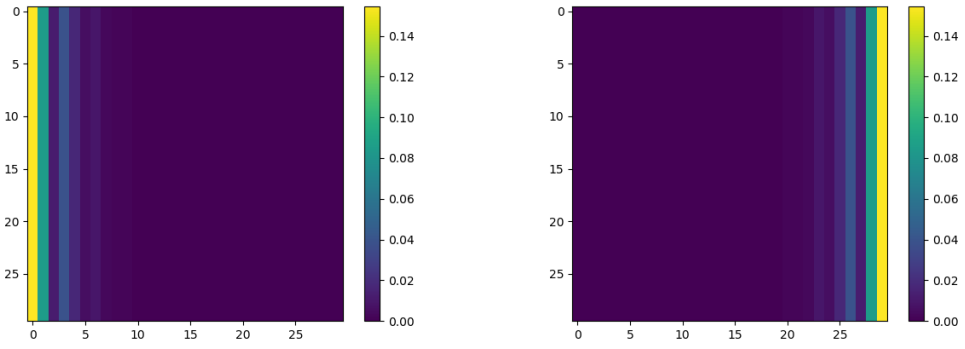

(a) (b)

Figure 8: Edge states for the ribbon geometry of the Haldane model. For display purposes, the color of each pixel represent the magnitude of the wavefunction for the entire fundamental cell, given by $\sqrt{(\psi^A)^2 + (\psi^B)^2}$.

states. It is called the *Chern number* and is defined as

$$C_\pm = \frac{1}{2\pi} i \int_0^{2\pi} \int_0^{2\pi} \frac{\partial}{\partial k_1} \langle \Phi_{00}(\pm, k_1, k_2) | \frac{\partial}{\partial k_2} \Phi_{00}(\pm, k_1, k_2) \rangle \\ - \frac{\partial}{\partial k_2} \langle \Phi_{00}(\pm, k_1, k_2) | \frac{\partial}{\partial k_1} \Phi_{00}(\pm, k_1, k_2) \rangle \, dk_1 dk_2, \quad (3.15)$$

where $\pm$ represent the plus or minus band in the eigenvalue spectrum (since we get two eigenvalues for each 2×2 matrix) and Φ_{00} represent the corresponding eigenvector for that band in the 0-th fundamental cell in both directions. The result of this integration is always an integer. If it is zero, then there are no edge states in the ribbon geometry with the same parameters. If it is nonzero, then edge states exist. The curve separating these two cases is given by equation 3.13 that we discussed. When $|V| < 3\sqrt{3}t' \sin\phi$, the Chern number is nonzero. When $|V| > 3\sqrt{3}t' \sin\phi$, the Chern number is zero. Using numerical integration, we were able to confirm the correctness of this relatioship. For points on the curve, however, the Chern number is not well-defined. We can see this by writing the Chern number in an equivalent way:

$$C_\pm = \frac{1}{2\pi} Im\left(\int_0^{2\pi} \int_0^{2\pi} \frac{\langle \Phi(\pm) | \frac{\partial}{\partial k_1} H \Phi(\mp) \rangle \langle \Phi(\mp) | \frac{\partial}{\partial k_2} H \Phi(\pm) \rangle)) - \langle \Phi(\pm) | \frac{\partial}{\partial k_2} H \Phi(\mp) \rangle) \langle \Phi(\mp) | \frac{\partial}{\partial k_1} H \Phi(\pm) \rangle}{(E_\pm(k_1, k_2) - E_\mp(k_1, k_2))^2} \right), \quad (3.16)$$

where $E_\pm$ is the eigenvalue in the plus or minus band. When we have degeneracy and the two bands touch, the denominator becomes zero, and the integrand goes to infinity. In such cases the Chern number cannot be used as a test for the existence of edge states because it is not defined. In all other cases, however, the Chern number, a bulk property, is associated with the existence of edge states, illustrating again the idea of bulk-boundary correspondence.

3.3 Time-reversal Symmetry

One interesting property of the edge states in the Haldane model is that the waves can travel only in a single direction. In our case, counterclockwise motion is allowed, but clockwise motion is not. This indicates the breaking of time-reversal symmetry of the system, meaning that reversing the arrow of time does not give a physically acceptable solution. This is a crucial characteristic of the edge states, and allows interesting behavior such as bypassing defects without reflection. Mathematically, time-reversal symmetry is defined to be

$$\overline{H(k_1, k_2)} = H(-k_1, -k_2). \quad (3.17)$$

When the Hamiltonian possesses this property, we see that

$$\begin{aligned} \overline{H(k_1,k_2)\Phi(k_1,k_2)} &= \overline{E(k_1,k_2)\Phi(k_1,k_2)} \\ H(-k_1,-k_2)\overline{\Phi(k_1,k_2)} &= E(k_1,k_2)\overline{\Phi(k_1,k_2)}. \end{aligned} \tag{3.18}$$

Thus, $\overline{\Phi(k_1,k_2)}$ is an eigenvector of $H(-k1,-k2)$. Taking the complex conjugate, in this case, is equivalent to flipping the direction of the crystal momenta k_1 and k_2. Thus, Equation 3.17 implies that the system allows a solution traveling in the reverse direction when we reverse the arrow of time, which is what time-reversal symmetry means.

Surprisingly, the Chern number is related to time-reversal symmetry by the following theorem

Theorem. *When a system possesses time-reversal symmetry, the Chern number for that system is zero.*

We can see that this is true by rewriting the Chern number in yet another way:

$$C = \frac{1}{2\pi}\int_{-\pi}^{\pi}\int_{-\pi}^{\pi} \frac{\partial}{\partial k_1}\langle\Phi|i\frac{\partial}{\partial k_2}\Phi\rangle - \frac{\partial}{\partial k_2}\langle\Phi|i\frac{\partial}{\partial k_1}\Phi\rangle\, dk_1 dk_2, \tag{3.19}$$

where Φ is the eigenvector of one particular band. From time-reversal symmetry, we know that

$$\Phi(-k_1,-k_2) = \overline{\Phi(k_1,k_2)}, \tag{3.20}$$

where $\Phi(-k_1,-k_2)$ is the eigenvector of $H(-k_1,-k_2)$. Looking at the first term of the integrand, we see that

$$\begin{aligned} \frac{\partial}{\partial k_1}\langle\Phi(k_1,k_2)|i\frac{\partial}{\partial k_2}\Phi(k_1,k_2)\rangle &= \frac{\partial}{\partial k_1}\langle\overline{\Phi(-k_1,-k_2)}|i\frac{\partial}{\partial k_2}\overline{\Phi(-k_1,-k_2)}\rangle \\ &= -\overline{\frac{\partial}{\partial k_1}\langle\Phi(-k_1,-k_2)|i\frac{\partial}{\partial k_2}\Phi(-k_1,-k_2)\rangle}. \end{aligned} \tag{3.21}$$

Notice that $\langle\Phi|\partial_{k_2}\Phi\rangle$ is imaginary. Since $\langle\Phi|\Phi\rangle = 1$ from normalization, we have $\partial_{k_2}\langle\Phi|\Phi\rangle = 0$. Expanding this, we get

$$\begin{aligned} \langle\partial_{k_2}\Phi|\Phi\rangle + \langle\Phi|\partial_{k_2}\Phi\rangle &= 0, \\ \overline{\langle\Phi|\partial_{k_2}\Phi\rangle} &= 0, \\ Re(\langle\Phi|\partial_{k_2}\Phi\rangle) &= 0. \end{aligned} \tag{3.22}$$

Thus, $\langle\Phi|i\partial_{k_2}\Phi\rangle$ is real. Applying this to Equation 3.21, we get

$$\frac{\partial}{\partial k_1}\langle\Phi(k_1,k_2)|i\frac{\partial}{\partial k_2}\Phi(k_1,k_2)\rangle = -(\frac{\partial}{\partial k_1}\langle\Phi(-k_1,-k_2)|i\frac{\partial}{\partial k_2}\Phi(-k_1,-k_2)\rangle). \tag{3.23}$$

This means that the first term of the integrand is an odd function. Similary, we can show that the second term is odd, too. Since the integration runs from $-\pi$ to π, the Chern number resulting from this integration is zero. This is an important theorem because it shows that edge states do not exist in the Haldane model when time-reversal symmetry is not broken. As we will see in Floquet topological insulators, generating edge states generally involves introducing a periodic driving that has some chirality, and thus breaks the time-reversal symmetry of the system.

4 The Floquet System and Time-dependent Hamiltonian

In the previous sections, we discussed the topological insulators whose corresponding Schrödinger equation has time-independent Hamiltonian. But, in fact, "true" topological insulators are not only difficult to find in nature or synthesize, but also hard to predict which substances may exhibit such properties. As Haldane model proved the possibility of natural topological insulator materials without utilizing quantum Hall effect, scientists further discovered that by adding a time varying

perturbation, a generic insulator could behave like a topological insulator. The system could be interpreted with the following general Schrödinger equation:

$$i\partial_t \psi = H(t)\psi, \text{where } H(t+T) = H(t), \forall t. \tag{4.1}$$

This time-periodic driving, which breaks the time-reversal symmetry, led to the experimental realization of some photonic Floquet topological insulators in the past few years and very likely other possibilities in the nearby future. We will discuss this with more examples in section 5. In this section, we will focus on a simple Floquet model brought up by Rudner et al. [6], and its properties in comparison with the time-independent Hamiltonian systems.

4.1 The Rudner Model

The Rudner Model depicts a simple two-dimensional lattice structured in figure 9, where the grey rectangle represents the fundamental cell that contains A and B sites. The hopping amplitudes are changing in a time-periodic way.

*(Another tikz inserted here and described, the direction, amplitude of the hopping and the onsite-potential, explain the hopping with figure 10a) When $\frac{4}{5}T \leq t < T$, all of the hopping terms are "turned off."

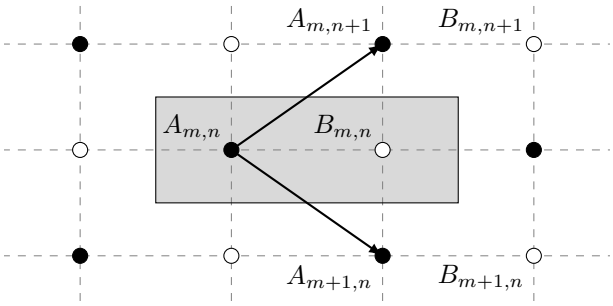

Figure 9: Lattice Structure in Rudner Model

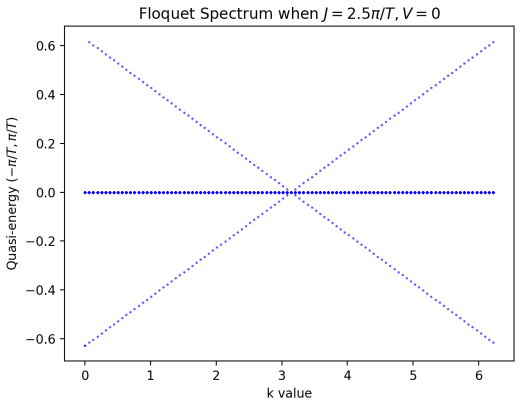

(a)

Figure 10: Floquet Spectrum when V = 0

This is modeled by the following Hamiltonian and V is the sublattice potential:

$$(H(t)\psi)_{m,n} = -\begin{pmatrix} J_1(t)\psi^B_{m,n} + J_2(t)\psi^B_{m-1,n} + J_3(t)\psi^B_{m-1,n-1} + J_4(t)\psi^B_{m,n-1} \\ J_1(t)\psi^A_{m,n} + J_2(t)\psi^A_{m+1,n} + J_3(t)\psi^A_{m+1,n+1} + J_4(t)\psi^A_{m,n+1} \end{pmatrix} + V\begin{pmatrix} \psi^A_{m,n} \\ -\psi^B_{m,n} \end{pmatrix}. \tag{4.2}$$

where:

$$J_n(t) = \begin{cases} J, & (n-1)\frac{T}{5} \leq t < n\frac{T}{5} \\ 0, & \text{otherwise} \end{cases}, n = 1, 2, 3, 4 \tag{4.3}$$

For $t \geq T$, $H(t)$ is defined as $H(t+T) = H(t)$, $\forall t$

Notice that this Floquet system cannot be solved by the method of eigenvector expansion and the superposition of the stationary state solutions, which are used in solving the SHH and Haldane models. Let $\Phi(t)$ and $E(t)$ denote the instantaneous eigenvectors and eigenvalues diagonalized from the time-dependent Hamiltonian $H(t)$. If the old method could still be implemented, the following should give the solution to the time-dependent Schrödinger equation 4.1:

$$\psi(t) = \sum \langle \Phi(t) | \, |\psi(0)\rangle \, \Phi(t) e^{-iE(t)t} \tag{4.4}$$

Because $\langle \Phi(t) | \, |\psi(0)\rangle \, \Phi(t)$ is t-dependent, we need to apply chain rule to compute $i\partial_t \psi(t)$. Given that $H(t)\psi(t) = E(t)\psi(t)$, calculation with chain rule will leave extra terms that could not be canceled from the other side of the equation. Therefore, we need to Floquet theory to analyze the system.

4.2 Floquet Theory

In this case, we can write the Schrödinger equation as:

$$i\partial_t \psi = H(t)\psi \iff (i\partial_t - H(t))\psi = 0, \tag{4.5}$$

which indicates that the solutions of the Schrödinger equation can be viewed as eigenvectors of the operator $i\partial_t - H(t)$ with eigenvalue 0. Define τ to be the time translation operator that translates functions of time by T:

$$(\tau\psi)(t) = \psi(t+T) \tag{4.6}$$

Similar to how we prove Bloch theory in section 2.2, given that the operator $H(t)$ is periodic, τ commutes with $i\partial_t - H(t)$. Thus, we can choose solutions of the Schrödinger equation which are simultaneously eigenvectors of the time-translation operator:

$$\psi(t+T) = Z\psi(t) \tag{4.7}$$

Since Schrödinger equation preserves normalization, we have:

$$|Z| = 1 \tag{4.8}$$

which can be described as:

$$Z = e^{-i\epsilon T}, \text{ for some real } \epsilon \in [-\frac{\pi}{T}, \frac{\pi}{T}) \tag{4.9}$$

ϵ is called the quasi-energy as opposed to the eigenvalue E of the time-independent Hamiltonian that called energy. Quasi-energy is the natural mathematical generalization of the energy to the Floquet systems. It tells us how the solutions behave after each period. The associated eigenvector is written as: $\Phi(t, \epsilon)$.

Generally speaking, because the Schrödinger equation is linear, we can also write its solution as $\psi(t_2) = U(t_2, t_1)\psi(t_1)$ where U is the unitary time evolution operator, or the propagator, that solves the time-dependent Schrödinger equation as the wave propagates. It is equal to identity matrix at the inital time:

$$U(t_2, t_1) = \mathcal{T} \exp\left(-i \int_{t_1}^{t_2} H(t) dt\right) \tag{4.10}$$

where $\mathcal{T}$ is the time-ordering operator. It is necessary if Hamiltonians evaluated at different times in the integral do not commute and the propagator thus satisfies the following multiplication rule:

$$U(t_3, t_1) = U(t_3, t_2)U(t_2, t_1) \tag{4.11}$$

In order to compute ϵ, we have to focus on the propagator which maps the initial conditions to the solution of the Schrödinger equation after one period: $U(T) : \psi(0) \mapsto \psi(T)$. Therefore, we can

find ϵ and the solutions by finding the associated eigenvalues λ and eigenvectors $\Phi(0,\epsilon)$ of $U(T)$, as they satisfy the following:

$$\Phi(T,\epsilon) = U(T)\Phi(0,\epsilon) = \lambda\Phi(0,\epsilon) \tag{4.12}$$

where

$$\lambda = e^{-i\epsilon T} \iff \epsilon = iT^{-1}\log\lambda \tag{4.13}$$

In Rudner Model, the propagator over one period T is calculated by multiplying the propagators over each interval $0 \le t < \frac{T}{5}$, $\frac{T}{5} \le t < \frac{2T}{5}$, ... together, *i.e.*,

$$U(T) = U_5U_4U_3U_2U_1 \tag{4.14}$$

where

$$U_n = e^{-iH_n\frac{T}{5}}\ ,\ H_n = H(t) \text{ in the interval } (n-1)\frac{T}{5} \le t < n\frac{T}{5} \tag{4.15}$$

4.3 Effective Hamiltonian Approach

In the time-independent Hamiltonian system, all the information, such as the solutions of the Schrödinger equation and the edge states, is contained in the eigenvalues and eigenvectors of the Hamiltonian. For the time-periodically driven system, we have to solve for the propagator $U(T)$ over the period for the corresponding generalization from what we called the effective Hamiltonian.

Recall from equation 4.12, we have:

$$\Phi(T,\epsilon) = e^{-i\epsilon T}\Phi(0,\epsilon) \tag{4.16}$$

where $\Phi(0,\epsilon)$ is the eigenvector of $U(T)$ with eigenvalue $e^{-i\epsilon T}$. Thus,

$$\Phi(2T,\epsilon) = e^{-i\epsilon T}\Phi(T,\epsilon) = e^{-i\epsilon(2T)}\Phi(0,\epsilon) \tag{4.17}$$

Therefore, at every integer multiple of T, we have:

$$\Phi(nT,\epsilon) = e^{-i\epsilon(nT)}\Phi(0,\epsilon) \tag{4.18}$$

In other words, if we ignore the periodic behavior of the system and observe "stroboscopically," *i.e.*, only look at $t = nT$, $n = 1, 2, ...$, the Floquet states behave like ordinary stationary states with energy ϵ. We can thus construct a time-independent Hamiltonian, called the effective Hamiltonian, whose stationary states behaves the same with the Floquet states at $t = 0, T, 2T, 3T...$:

$$H_{\text{eff}} := iT^{-1}\log(U(T)) \tag{4.19}$$

Given that $U(T)$ is a unitary matrix, let V denote the matrix whose columns are the eigenvectors of $U(T)$, so that $U(T) = VDV^*$ where D is diagonal:

$$D = \begin{pmatrix} \lambda_1 & & & \\ & \lambda_2 & & \\ & & \ddots & \\ & & & \lambda_n \end{pmatrix} \tag{4.20}$$

Then:

$$\log(U(T)) = V\log(D)V^* = V\begin{pmatrix} \log(\lambda_1) & & & \\ & \log(\lambda_2) & & \\ & & \ddots & \\ & & & \log(\lambda_n) \end{pmatrix}V^* \tag{4.21}$$

The eigenvalues of this H_{eff} are the quasi-energies and the corresponding eigenvectors are called the Floquet states. We will discuss more in section 4.4.

*(Notice that the propagators for times in between the multiple integer of T will not be the same.)

4.4 Quasi-energy and Floquet Spectra

When we solve for the effective Hamiltonian, we start from the discrete time-evolution, where we only look at the state of the system $t = 0, T, 2T, 3T, ...$ and then apply the same unitary operator $U(T)$ each time to move the system forward through these discrete time steps. In this way, the effective Hamiltonian plays an analogous role to the Hamiltonian in a non-driven system. Therefore, if I expand the corresponding eigenvectors of H_{eff} and apply the same superposition method, we can also obtain information regarding the properties of the system. The corresponding eigenvalues of H_{eff}, the quasi-energies, will play an analogous role too in telling us how the system evolves once we ignore its periodic behavior.

Figure 13 show the Floquet spectra of the Rudner Model when varying J and V within the ribbon geometry context. Because of the periodicity of the quasi-energy in the Floquet system, there is one edge state in figure 12c near $\epsilon = \frac{\pi}{T}$, two edges in figure 12c near $\epsilon = \frac{\pi}{T}$ and 0, and no edge state in figure 12a.

Similarly to how we find the edge states in the Haldane Model, if we select the eigenvectors at the anomalous edge state and expanded them into full 2D matrices with one-way periodic Bloch's theory, we will get two edge states with respect to each edge in the ribbon geometry. Figure 11 gives an example of two edge states around quasi-energy $\epsilon = 0$ when $J = 2.5\frac{\pi}{T}$ and $V = 0.5\frac{\pi}{T}$.

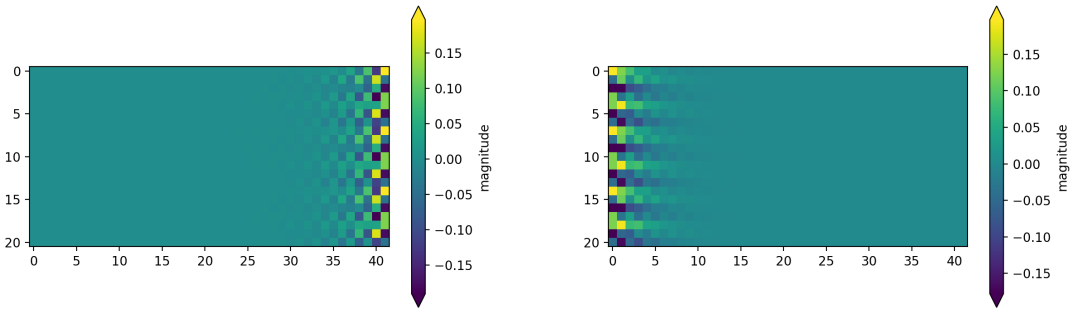

(a) (b)

Figure 11: Two Floquet Anomalous Edge States After Eigenvector Expansion

4.5 $W_3[U_\xi]$ Invariant

While both the effective Hamiltonian and the Floquet spectra give us nice basis on importing some of the ideas of topological classification from non-driven systems into the context of periodically-driven systems, the differences between both systems remain significant as well.

Chern number is considered as one of the most important topological invariants in terms of the property of the topological insulators; however, it is not as effective as we expect it to be when it comes to the Floquet system. In a non-driven system, we can perceive its band structure as living in a cylinder because the periodic k value can be parametrized into a circle. In a periodically driven system, in addition to the periodic k value, the energy-like quasi-energy is itself periodic, which leads to torus-like infinite bank structure, meaning that the spectrum values at $-\frac{\pi}{T}$ is connected with that of $\frac{\pi}{T}$. Because of this different topology of the surface that the spectrum lives on, the topological classification of these systems is different as well. This gives rise to phenomenon that can be uniquely observed in Floquet systems, but not in non-driven systems. For example, figure 12e gives the Chern numbers 0 for both bands, as also showed in table 1. If we are considering in a non-driven system, we would expect no edge states; however, we do observe edge states in the periodically driven Rudner model, as indicated by the W_3 invariant.

In Floquet systems where the band structure lives in a torus, time periodically, W_3 invariant

can give the number of the anomalous edge states that cannot be predicted by other invariants such as the Chern number of the Floquet bands, which is directly related with the eigenvalues of the the unitary map U as defined in equation 4.2 [6].

In the trivial case of the Floquet system where U is periodic in the t direction, meaning that $U(T) \neq U(0) = I$, W_3 can be defined by:

$$W_3 = \frac{1}{8\pi^2} \int \mathrm{Tr}(U^{-1}\partial_t U[U^{-1}\partial_{k_1} U, U^{-1}\partial_{k_2} U])dtdk_1dk_2. \tag{4.22}$$

Moreover, the computation method is different for both the Chern number and the W_3 invariant in the general Floquet systems compared with those of in Haldane and SHH models. Because numerically, as we constructed the unitary map $U : \mathbb{T}^3 \to \mathbb{U}(n)$ within a discretized grid of discrete values, we can no longer get the partial derivatives required in the continuous formulas for the W_3 computation (same with the Chern number computation [2]). Thus, we use an efficient computation method to approximate W_3 [4]. Notice that because the Floquet systems are not periodic in the t direction, the general computation for W_3 is not accurate and requires a correction term dependent on a variable ξ, a value picked in the range of the quasi-energy (normally chosen as $-\frac{\pi}{T}$, $\frac{\pi}{T}$) as showed in figure 13:

$$W_3[U_\xi] = W_3 + \text{correction}(\xi) \tag{4.23}$$

The value of $W_3[U_\xi]$ therefore gives the number of anomalous edge states with respect to the certain ξ.

$W_3[U_\xi]$ is more accurate in determining the edge states, if compared with the Chern number of the two Floquet bands using a similar efficient discretized computation method. See table 1 below:

J	V	Chern Number		W_3 Invariant	
$0.5\frac{\pi}{T}$	$0.5\frac{\pi}{T}$	+ band	0	$\xi = \pi/T$	0
		− band	0	$\xi = 0$	0
$1.5\frac{\pi}{T}$	$0.5\frac{\pi}{T}$	+ band	1	$\xi = \pi/T$	1
		− band	-1	$\xi = 0$	0
$2.5\frac{\pi}{T}$	$0.5\frac{\pi}{T}$	+ band	0	$\xi = \pi/T$	1
		− band	0	$\xi = 0$	1

Table 1: Chern Number and W_3 Invariant Comparison

5 From Tight Binding to PDE

5.1 Tight-Binding Polarized Light with Graphene Model

We now examine the tight-binding model for graphene when polarized light is added. Recall that the Hamiltonian for graphene is given by

$$H = \begin{pmatrix} 0 & t(1 + e^{-ik_1} + e^{-ik_2}) \\ t(1 + e^{ik_1} + e^{ik_2}) & 0 \end{pmatrix}. \tag{5.1}$$

In order to account for the addition of the light to this model, we add an extra term so that the Hamiltonian becomes.

$$H = \begin{pmatrix} 0 & t(1 + e^{-ik_1} + e^{-ik_2}) + A_0 \sin(\omega t) \\ t(1 + e^{ik_1} + e^{ik_2}) + A_0 \sin(\omega t - \phi) & 0 \end{pmatrix}. \tag{5.2}$$

Here, A_0 represents the amplitude of the light, ω is the frequency of light, and ϕ is the phase of the light to allow for different polarizations. Since circularly polarized light will lead to the properties of a topological insulator, we need to set the phase to be $\frac{\pi}{2}$. Since the hamiltonian for this model varies continously with time, we take a discrete sampling of the model to make this model discrete like the Rudner model. Using this model, and analyzing the model with the same method as the Rudner Model, we get the Floquet spectra and winding number diagrams shown in the figure below. We can see that the winding number still remains accurate in predicting the number of edge states in the Polarized Light and Graphene model.

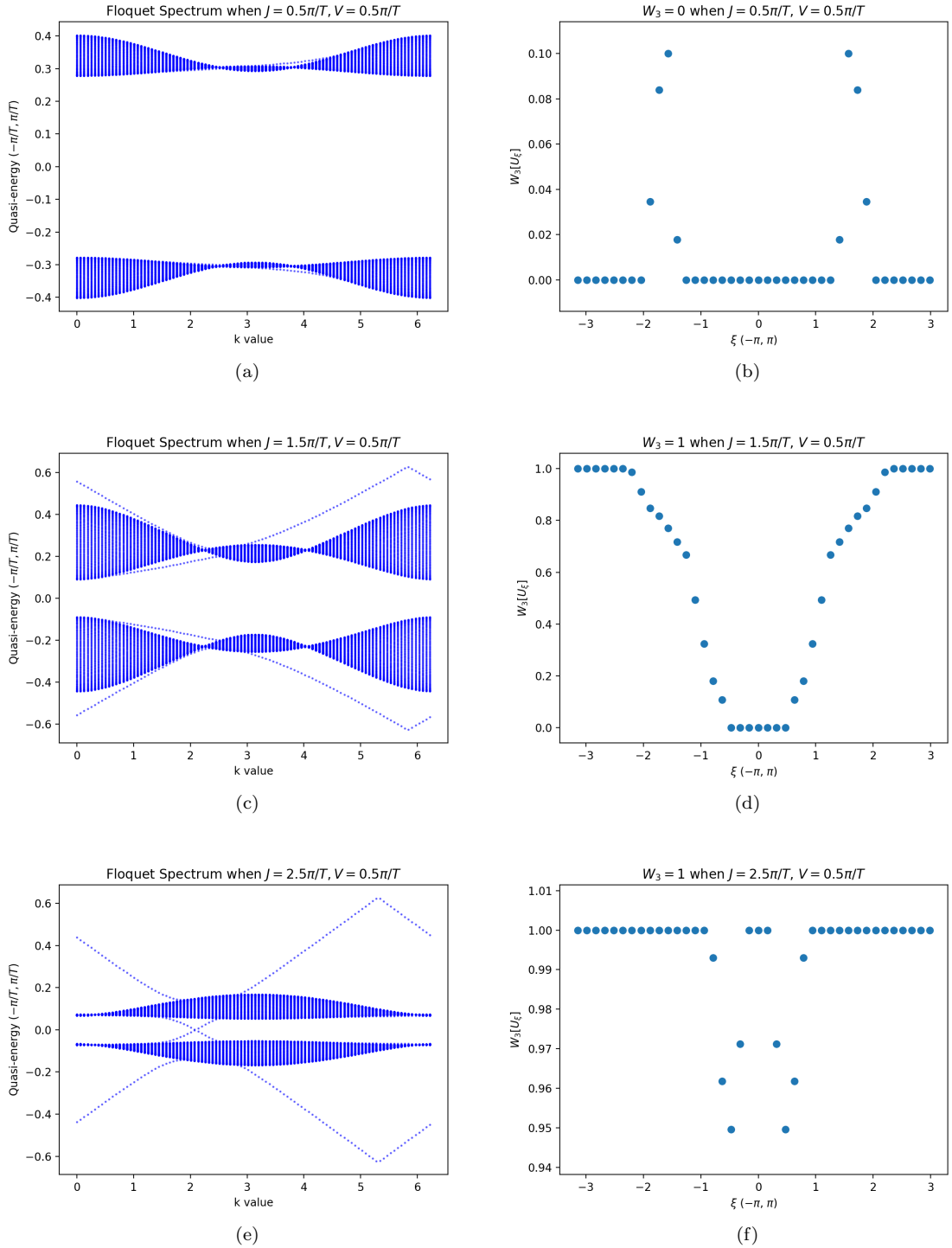

Figure 12: Floquet Spectra and $W_3[U_\xi]$ Computations of the Rudner Model

5.2 PDE Model

We shall now examine the PDE model for graphene. The main difference between this model and the tight-binding models that we have previously examined is that the tight-binding models assume that electrons hop between the two sites on each fundamental cell, while the PDE model does not make this assumption. Due to this, electrons may be found anywhere in each fundamental cell in

this model, and not just at the A and B sites.
As mentioned before, each fundametal cell of graphene lies on a hexagonal lattice defined by the vectors

$$\vec{v}_1 = \frac{1}{2}(3, -\sqrt{3}), \vec{v}_2 = \frac{1}{2}(3, \sqrt{3}), \tag{5.3}$$

with the distance between the A and B site in each cell being defined by

$$\vec{e}_1 = (1, 0). \tag{5.4}$$

The Hamiltonian operator for this system is the usual time-independent operator in two spatial dimensions defined to be

$$H = -\frac{1}{2}\left(\frac{\partial^2}{\partial x^2} + \frac{\partial^2}{\partial y^2}\right) + V(x, y). \tag{5.5}$$

where $V(x, y)$ represents the potential. It is represented as two finite wells with centers located at $(1, 0)$ and $(2, 0)$.
We also assume that the material is an infinite sheet, so we may apply Bloch theory to also get the relationships

$$\Phi(\vec{r} + \vec{v}_1) = e^{ik_1}\Phi(\vec{r}) \tag{5.6}$$

$$\Phi(\vec{r} + \vec{v}_2) = e^{ik_2}\Phi(\vec{r}) \tag{5.7}$$

where $\vec{r} = (x, y)$. We would like to be able to discretize this problem by dividing the fundamental cell into a grid, and analyzing Schrodinger's equation at each point on the grid; however, the standard basis that we normally use to define graphene does not give us any such easy division. Thus, we use a different basis to analyze the equation. Specifically, we use the basis composed of the vectors $v = (\vec{v}_1, \vec{v}_2)$ that are used to translate each fundamental cell. We shall refer to the coordinates in this basis as $(\tilde{x}, \tilde{y})$, which can easily be seen as

$$\vec{r} = x \cdot \vec{e}_1 + y \cdot \vec{e}_2 = \tilde{x} \cdot \vec{v}_1 + \tilde{y} \cdot \vec{v}_2. \tag{5.8}$$

It is clear that the change of basis matrix from $v = (\vec{v}_1, \vec{v}_2)$ to $e = (\vec{e}_1, \vec{e}_2)$ is given by

$$[T]_v^e = \begin{pmatrix} \frac{3}{2} & \frac{3}{2} \\ -\frac{\sqrt{3}}{2} & \frac{\sqrt{3}}{2} \end{pmatrix} \tag{5.9}$$

The change of basis matrix from $e = (\vec{e}_1, \vec{e}_2)$ to $v = (\vec{v}_1, \vec{v}_2)$ is given by the inverse,

$$[T]_e^v = \begin{pmatrix} \frac{1}{3} & -\frac{\sqrt{3}}{3} \\ \frac{1}{3} & \frac{\sqrt{3}}{3} \end{pmatrix} \tag{5.10}$$

Now that we have found a basis that is easy to divide, we must now actually divide the basis into a grid to analyze. We do this as shown in Figure . We divide the square formed by the fundamental cell in basis v into a grid with a spacing of h between each adjacent point in both directions, with the total number of points being $\frac{1}{h}\frac{1}{h} = \frac{1}{h^2}$.
In the actual discretization of Schrodinger's Equation we will examine each grid point as a component of the overall wavefunction such that

$$\psi = \begin{pmatrix} \psi_{0,0} \\ \psi_{0,h} \\ \psi_{0,2h} \\ \vdots \\ \psi_{0,1-h} \\ \psi_{1,0} \\ \psi_{1,h} \\ \vdots \\ \psi_{1-h,1-h} \end{pmatrix} \tag{5.11}$$

We now need to determine how to rewrite Equation 5.3, Schrodinger's equation in terms of $(\tilde{x}, \tilde{y})$.

In order to rewrite the Laplacian in terms of $\tilde{x}$ and $\tilde{y}$, we use the chain rule,

$$\frac{\partial^2}{\partial x^2} = \left(\frac{\partial \tilde{x}}{\partial x}\right)^2 \frac{\partial^2}{\partial \tilde{x}^2} + 2\frac{\partial \tilde{x}}{\partial x}\frac{\partial \tilde{y}}{\partial x}\frac{\partial^2}{\partial \tilde{x}\partial \tilde{y}} + \left(\frac{\partial \tilde{y}}{\partial x}\right)^2 \frac{\partial^2}{\partial \tilde{y}^2} \tag{5.12}$$

$$\frac{\partial^2}{\partial y^2} = \left(\frac{\partial \tilde{x}}{\partial y}\right)^2 \frac{\partial^2}{\partial \tilde{x}^2} + 2\frac{\partial \tilde{x}}{\partial y}\frac{\partial \tilde{y}}{\partial y}\frac{\partial^2}{\partial \tilde{x}\partial \tilde{y}} + \left(\frac{\partial \tilde{y}}{\partial y}\right)^2 \frac{\partial^2}{\partial \tilde{y}^2} \tag{5.13}$$

Substituting the values for the derivatives that we have from the change of basis matrix gives us the Laplacian to be

$$\frac{\partial^2}{\partial x^2} + \frac{\partial^2}{\partial y^2} = \frac{4}{9}\frac{\partial^2}{\partial \tilde{x}^2} - \frac{4}{9}\frac{\partial^2}{\partial \tilde{x}\partial \tilde{y}} + \frac{4}{9}\frac{\partial^2}{\partial \tilde{y}^2} \tag{5.14}$$

In the same manner, we can also write the potential as

$$V(x,y) = \begin{cases} V & \text{if } \sqrt{\frac{3}{2}(\tilde{x}+\tilde{y}-1)^2 + \frac{\sqrt{3}}{2}(\tilde{y}-\tilde{x})^2} \leq 0.1 \\ V & \text{if } \sqrt{\frac{3}{2}(\tilde{x}+\tilde{y}-2)^2 + \frac{\sqrt{3}}{2}(\tilde{y}-\tilde{x})^2} \leq 0.1 \\ 0 & \text{otherwise} \end{cases} \tag{5.15}$$

Now that we have the Laplacian in terms of $\tilde{x}$ and $\tilde{y}$, we can use the theory of finite differences to estimate the derivative at the various points. We use the central difference approximations given by

$$\frac{\partial^2 \psi}{\partial \tilde{x}^2} = \frac{\psi(\tilde{x}+h,\tilde{y}) - 2\psi(\tilde{x},\tilde{y}) + \psi(\tilde{x}-h,\tilde{y})}{h^2} \tag{5.16}$$

$$\frac{\partial^2 \psi}{\partial \tilde{y}^2} = \frac{\psi(\tilde{x},\tilde{y}+h) - 2\psi(\tilde{x},\tilde{y}) + \psi(\tilde{x},\tilde{y}-h)}{h^2} \tag{5.17}$$

$$\frac{\partial^2 \psi}{\partial \tilde{x}\partial \tilde{y}} = \frac{\psi(\tilde{x}+h,\tilde{y}+h) - \psi(\tilde{x}+h,\tilde{y}-h) - \psi(\tilde{x}-h,\tilde{y}+h) + \psi(\tilde{x}-h,\tilde{y}-h)}{4h^2} \tag{5.18}$$

We also include the periodicity given by Bloch's Theorem in the finite difference matrix. For example, $f(\tilde{x}-h,y)$ is not formally defined when $\tilde{x}=0$, however, due to Bloch's Theorem we may write this as

$$f(\tilde{x}-h,y) = f(1+\tilde{x}-h,y)e^{-ik_1} \tag{5.19}$$

An example finite difference matrix for $\frac{\partial^2 \psi}{\partial \tilde{x}^2}$ is given below with $h = \frac{1}{3}$.

$$\frac{\partial^2 \psi}{\partial \tilde{x}^2} = \begin{pmatrix} -2 & 0 & 0 & 1 & 0 & 0 & e^{-ik_1} & 0 & 0 \\ 0 & -2 & 0 & 0 & 1 & 0 & 0 & e^{-ik_1} & 0 \\ 0 & 0 & -2 & 0 & 0 & 1 & 0 & 0 & e^{-ik_1} \\ 1 & 0 & 0 & -2 & 0 & 0 & 1 & 0 & 0 \\ 0 & 1 & 0 & 0 & -2 & 0 & 0 & 1 & 0 \\ 0 & 0 & 1 & 0 & 0 & -2 & 0 & 0 & 1 \\ e^{ik_1} & 0 & 0 & 1 & 0 & 0 & -2 & 0 & 0 \\ 0 & e^{ik_1} & 0 & 0 & 1 & 0 & 0 & -2 & 0 \\ 0 & 0 & e^{ik_1} & 0 & 0 & 1 & 0 & 0 & -2 \end{pmatrix} \tag{5.20}$$

Now that we have discretized each of the components of Schrodinger's equation, we may now compute the eigenvalues of the matrix equation. As we did in the tight-binding model, we compute the eigenvalues over the Floquet spectrum, as shown in Figure 14. Looking at the lowest two energy bands, as shown in Figure 14, we can see that the tight-binding model does indeed give a good approximation for the PDE model for both the torus and ribbon geometry.

Future work involving this model will include creating a PDE model of graphene with the polarized light added, which will allow us to also validate that the methods we used are also accurate for that model as well.

References

[1] János K Asbóth, László Oroszlány, and András Pályi. "A short course on topological insulators". *Lecture notes in physics* 919 (2016).

[2] Takahiro Fukui, Yasuhiro Hatsugai, and Hiroshi Suzuki. "Chern Numbers in Discretized Brillouin Zone: Efficient Method of Computing (Spin) Hall Conductances". *Journal of the Physical Society of Japan* 74.6 (2005), pp. 1674–1677.

[3] F Duncan M Haldane. "Model for a quantum Hall effect without Landau levels: Condensed-matter realization of the" parity anomaly"". *Physical review letters* 61.18 (1988), p. 2015.

[4] B Höckendorf, A Alvermann, and H Fehske. "Efficient computation of the W 3 topological invariant and application to Floquet–Bloch systems". *Journal of Physics A: Mathematical and Theoretical* 50.29 (2017), p. 295301.

[5] T. Kitagawa, T. Oka, A. Brataas, L. Fu, and E. Demler. "Transport properties of nonequilibrium systems under the application of light: photoinduced quantum Hall insulators without Landau levels". *Phys. Rev. B* 84.23 (2011), p. 235108.

[6] M. S. Rudner, N. H. Lindner, E. Berg, and M. Levin. "Anomalous Edge States and the Bulk-Edge Correspondence for Periodically Driven Two-Dimensional Systems". *Phys. Rev. X* 3 (3 2013), p. 031005.

[7] W. P. Su, J. R. Schrieffer, and A. J. Heeger. "Solitons in Polyacetylene". *Phys. Rev. Lett.* 42.25 (1979), pp. 1698–1701.

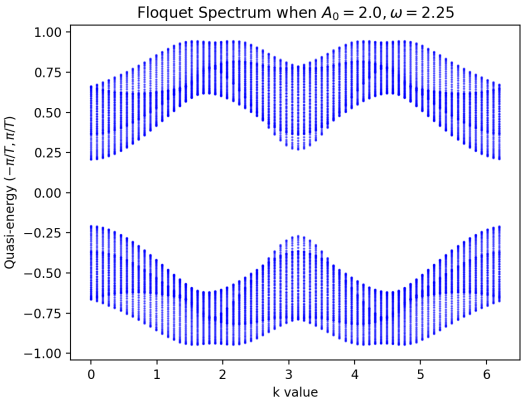
Floquet Spectrum when $A_0 = 2.0, \omega = 2.25$
Quasi-energy $(-\pi/T, \pi/T)$
k value

(a)

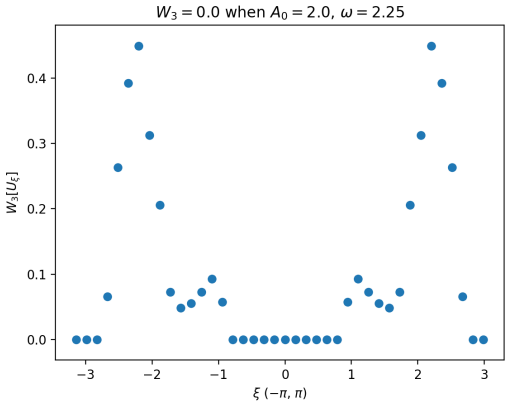
$W_3 = 0.0$ when $A_0 = 2.0, \omega = 2.25$
$W_3[U_\xi]$
$\xi\ (-\pi, \pi)$

(b)

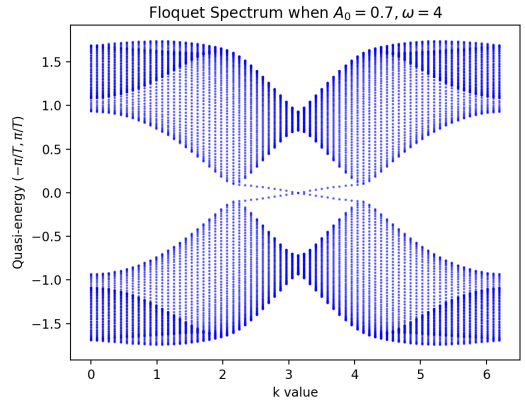
Floquet Spectrum when $A_0 = 0.7, \omega = 4$
Quasi-energy $(-\pi/T, \pi/T)$
k value

(c)

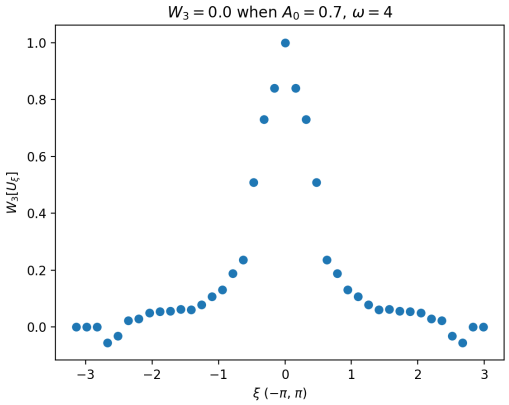
$W_3 = 0.0$ when $A_0 = 0.7, \omega = 4$
$W_3[U_\xi]$
$\xi\ (-\pi, \pi)$

(d)

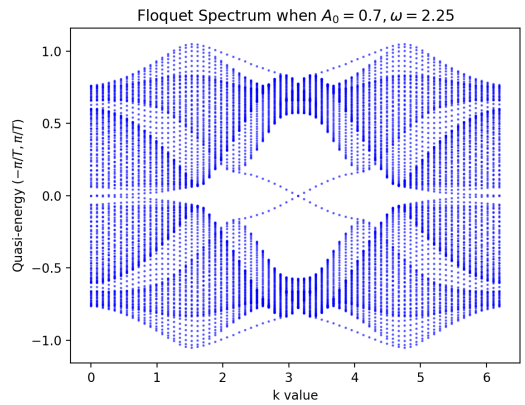
Floquet Spectrum when $A_0 = 0.7, \omega = 2.25$
Quasi-energy $(-\pi/T, \pi/T)$
k value

(e)

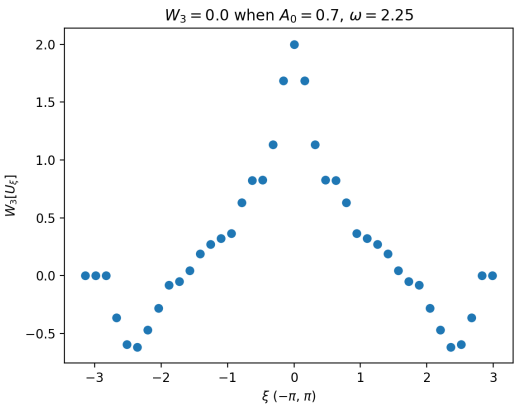
$W_3 = 0.0$ when $A_0 = 0.7, \omega = 2.25$
$W_3[U_\xi]$
$\xi\ (-\pi, \pi)$

(f)

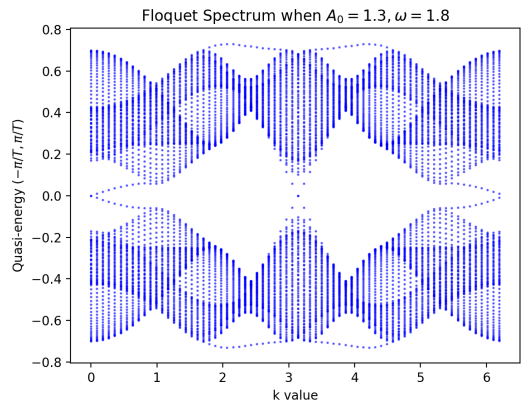
Floquet Spectrum when $A_0 = 1.3, \omega = 1.8$
Quasi-energy $(-\pi/T, \pi/T)$
k value

(g)

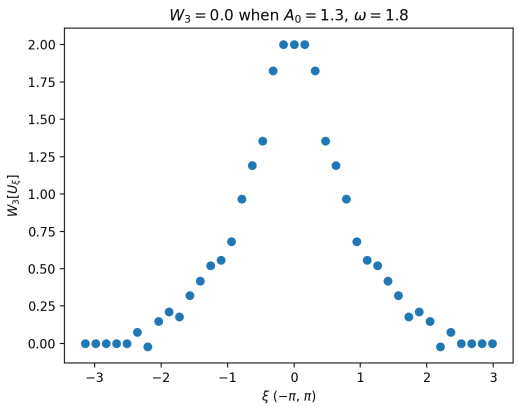
$W_3 = 0.0$ when $A_0 = 1.3, \omega = 1.8$
$W_3[U_\xi]$
$\xi\ (-\pi, \pi)$

(h)

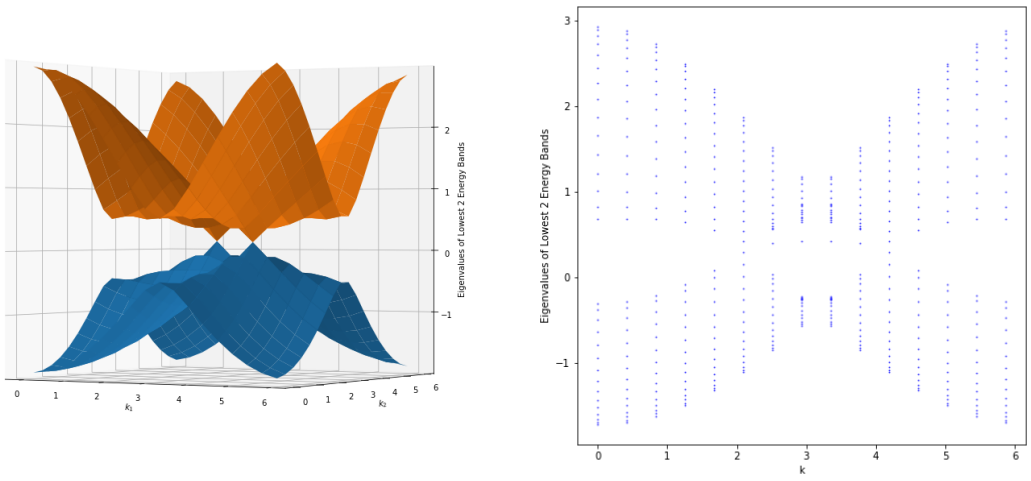

(a) (b)

Figure 14: Eigenvalue Spectrum of the Torus and Ribbon Geometry cases of Graphene